Biosensors and Bioelectronics 25 (2009) 488–492

Contents lists available at ScienceDirect

Biosensors and Bioelectronics

journal homepage: www.elsevier.com/locate/bios

Short Communication

A novel strategy for rapid real-time chiral discrimination of enantiomers using serum albumin functionalized QCM biosensor

Wen Cui Su [a], Wei Guang Zhang [a,*], Sheng Zhang [b], Jun Fan [a], Xia Yin [a], Miao Li Luo [a], Siu Choon Ng [c,*]

[a] School of Chemistry & Environment, South China Normal University, Guangzhou 510006, PR China
[b] Department of Chemistry, National University of Singapore, 117543, Singapore
[c] Division of Chemical and Biomolecular Engineering, Nanyang Technological University, 637459, Singapore

ARTICLE INFO

Article history:
Received 16 April 2009
Received in revised form 23 June 2009
Accepted 26 June 2009
Available online 5 July 2009

Keywords:
QCM
Serum albumin
Biosensor
Chiral discrimination
UV/FL Spectra

ABSTRACT

A novel and effective method has been developed for chiral discrimination using a quartz crystal microbalance (QCM) biosensor with self-assembled bovine serum albumin (BSA) or human serum albumin (HSA). The successfully constructed QCM chiral biosensors exhibited rapid and real-time enantioselective recognition. The QCM chiral discrimination factor (α_{QCM}) can be calculated through resonance frequency shifts in response to five pairs of enantiomers. Moreover, the interactions between these ten enantiomers and two serum albumins (SA) were investigated in detail by means of ultraviolet–visible (UV–vis) and fluorescence (FL) spectra. The results indicated that the discrimination ability were quite different between BSA and HSA. *R*,*S*-1-(3-Methoxyphenyl)ethylamine (*R*,*S*-3-MPEA) and *R*,*S*-1-(4-methoxyphenyl)ethylamine (*R*,*S*-4-MPEA) can be easily differentiated by the BSA sensor, while the selectivity of the HSA sensor for *R*,*S*-tetrahydronaphthylamine (*R*,*S*-TNA), *R*,*S*-2-octanol (*R*,*S*-2-OT) and *R*,*S*-methyl lactate (*R*,*S*-MEL) was higher than that of the BSA sensor. The UV and FL spectra indicated the formation of a complex between SA and enantiomers and strong fluorescence quenching through static quenching mechanism. The in-depth study demonstrated that the calculated UV/FL discrimination factors (α_{UV} and α_{FL}) were consistent with the QCM experimental results (α_{QCM}).

1. Introduction

With the development of biological science and technology, the determination and separation of enantiomers, especially those of pharmaceutical importance, is essential because of the role of chirality in living systems (Ahuja, 2000). Each enantiomer may have different pharmacological functions from its mirror image, in terms of activity, potency, toxicity, transport mechanism and metabolic route. At present, various methods have been investigated for chiral separation, such as capillary electrophoresis, thin-layer chromatography, supercritical fluid chromatography, gas chromatography and high performance liquid chromatography (Ward, 2000; Wei et al., 2005; Sadik et al., 2009). Furthermore, QCM chiral sensor remains a challenge to achieve online analysis of enantiomeric compounds in both gas and liquid phase, which represents a promising analytical method in characterizing enantiomers, due to its rapid analysis speed, satisfactory sensitivity and low cost. Inagaki et al. have demonstrated the immobilization of three types of cyclodextrin chiral selectors onto QCM sensor electrodes and observed significant frequency changes towards different enantiomer samples. (Inagaki et al., 2008). In addition, ten chiral sensors immobilized with mercaptyl perfunctionalized-cyclodextrins exhibited the promising enantioselectivity to three pairs of enantiomers (*R*,*S*-methyl lactate, *R*,*S*-ethyl lactate and *R*,*S*-2-octanol) in the gas phase (Ng et al., 2008). Kim et al. have presented a new method for the highly selective recognition of chiral mandelic acid by L-phenylalanine-modified sensor using quartz crystal microbalance (Kim et al., 2009).

Living systems contain large numbers of biological macromolecules, among which proteins and enzymes show natural enantioselectivity. Serum albumins are the most abundant proteins in the circulatory system, which can maintain the normal plasma osmotic pressure. The special spherical structures comprising of three hydrophobic domains are specific to bind and transport numerous endogenous and exogenous substances by reversible non-covalent bonding (Kragh-Hansen et al., 2002; Feng et al., 2007; Li et al., 2007; Du et al., 2009).

However, the combination of biological macromolecules and QCM technique has hitherto been rarely reported for the studies of chiral discrimination and host-guest interactions. Accordingly, our group has embarked upon the designed a class of novel QCM chiral sensors with self-assembled BSA or HSA for real-time chiral recognition, and investigated the host-guest interactions by UV and FL spectra.

* Corresponding authors. Tel.: +862039310210; fax: +862039347768.
E-mail address: wgzhang@scnu.edu.cn (W.G. Zhang).

0956-5663/$ – see front matter © 2009 Elsevier B.V. All rights reserved.
doi:10.1016/j.bios.2009.06.040

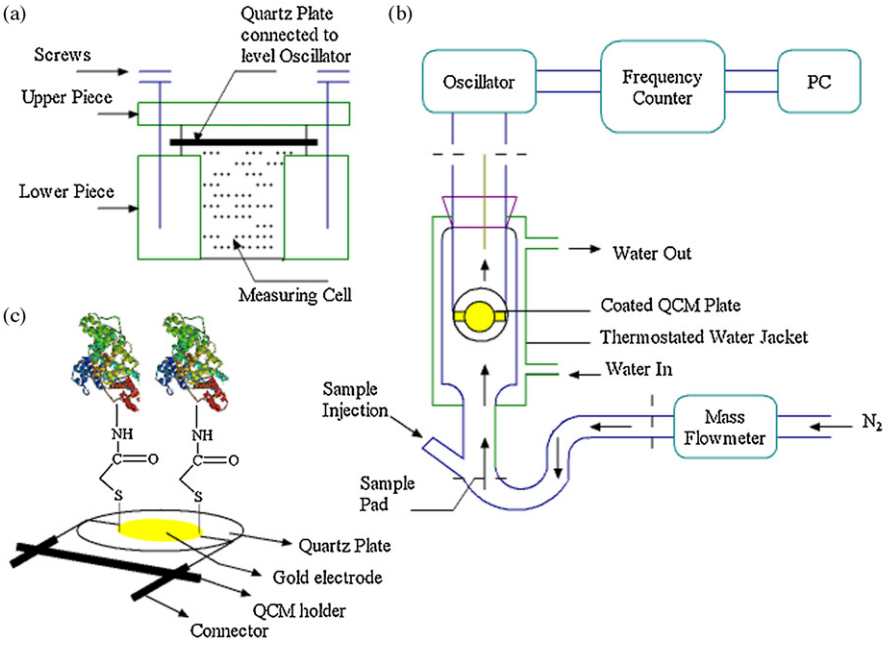

Fig. 1. A schematic view of the QCM systems. (a). Aqueous media measuring system. (b). Gas phase pulse-measuring system. (c). 10 MHz electrode quartz crystal.

2. Experimental

2.1. Materials and reagents

The structures of five pairs of enantiomers obtained from Alfa Aesar are shown in Fig. S1 in supplementary data. Both BSA and HSA were purchased from Hynost biotechnology Co., Ltd (Guangzhou, China). They were always prepared freshly in the buffer which consisted of 0.05 mol l^{-1} Tris-HCl and 0.1 mol l^{-1} NaCl, pH 7.4, and then were diluted to the experimental concentration. All other chemicals were of analytical grade and double distilled water was used throughout.

2.2. Apparatus and measurements

There are two home-made QCM systems (Fig. 1), (i): an aqueous media measuring system for monitoring the procedures of immobilization (Fig. 1a) and (ii): a gas phase pulse-measuring system for recognizing enantiomers (Fig. 1b). Each system consisted of a QCM sensor, a reaction cell, an oscillator detector, a frequency counter and a computer. The AT-cut quartz crystals (13.0 mm diameter, 10 MHz resonant frequency) were covered with gold electrodes on both sides (Fig. 1c).

In the gas phase pulse-measuring system, a vaporization pad allowed microscale enantiomeric samples to be evaporated. Predried pure nitrogen was used as carrier gas and the flow rate was controlled using an Alicat mass flow meter at 250 ± 2 ml min^{-1}.

The SA quartz crystal sensors were prepared by using a three-step assembling process in the aqueous media measuring system (Fig. S2, supplementary data) and the online frequency changes were recorded.

A 1.0×10^{-5} mol l^{-1} SA in Tris-HCl buffer (3.0 ml) was added accurately into a 1.0 cm quartz cell, and then titrated by successive additions of 1.0×10^{-2} mol l^{-1} each single enantiomer to attain a series of concentrations gradient. The UV absorption measurements were performed on a UV-1700 spectrophotometer (SHIMADZU, Japan) at the room temperature in the range from 230 to 320 nm. Fluorescence spectra were recorded on a FLS-920 spectrophotometer (EDINBURGH, England) from 285 to 450 nm.

3. Results and discussion

3.1. Formation of self-assembled monolayer of SA on quartz crystal

Immobilization of biological compounds onto Au surfaces using the self-assembled monolayer (SAM) techniques has been reported as one of the most promising and suitable techniques for coating layers (Storri et al., 1998; Fung and Wong, 2001; Akkerman et al., 2007; Cho et al., 2008; Silien et al., 2009; Malhotra et al., 2009). Thiol can be strongly adsorbed on the gold surface to afford stable and ordered layers due to the formation of covalent bonds between gold and sulfur, and the maximal bond energy could reach 184 kJ mol^{-1}. Accordingly, some short-chain thiol compounds, such as mercaptoacetic acid, were used to form a monolayer with free carboxylic acid terminal groups. The carboxylic groups can be activated by two coupling agents (EDC and NHS) to generate stable acylamino ester intermediates, so as to facilitate the adhesion of SA onto the gold surface.

The processes of carboxylic acid terminated monolayer activation and SA immobilization on Au surface have been monitored in the aqueous media measuring system (Fig. S3, supplementary data). The results showed that the oscillation frequency decreased quickly and reached equilibrium within 3 h after NHS and EDC solution was injected into the reaction cell. The processes were chemisorption rather than physisorption, as shown by the slight frequency rises when washed with buffer in order to remove excess reagents. It can be seen that the frequency of BSA ($\Delta f = -27$ Hz) decreased more than that of HSA ($\Delta f = -20$ Hz) immediately after immobilization, and then rose to -17 Hz and -14 Hz after rinsing with buffer. The differences might be related to the natural structures of the two proteins (Jacinto et al., 1971). The surface concentration of SA Θ can be calculated as the equation (Ng et al., 2008).

$$\Theta = k\frac{\Delta f}{M}, \quad (1)$$

where M is the molecular weight of chiral selector (BSA or HSA), $k = -4.42 \times 10^{-9}$ g Hz^{-1} cm^{-2}. And the surface concentration of BSA and HSA immobilized on the gold were 1.1×10^{-12} mol cm^{-2} and 0.9×10^{-12} mol cm^{-2}.

3.2. Real-time chiral discrimination of enantiomers by BSA and HSA sensor

The frequency changes were measured against time as each single enantiomer was injected into the gas system to interact with BSA (Fig. S4) and HSA (Fig. S5). The decreased frequency demonstrated interactions between enantiomers and SA, and the results were found reproducible over five consecutive measurements. The binding affinity of BSA and HSA for all five pairs of enantiomers was stereodependent. The *S*-enantiomer of TNA was preferred as indicated by the higher frequency shifts than the *R*-enantiomer. On the other hand, the *R*-enantiomers of the other four pairs were preferred. According to the "Lock-and-Key" mechanism (Cramer, 1994), the size, shape, and polarity of the host-guest molecules are the most critical factors influencing the stability of the inclusion complex. It is therefore believed that the hydrophobic cavities of SA preferred *R*- to *S*-enantiomer in case of 4-MPEA, 2-OT, MEL.

The effectiveness of the QCM sensor can be well described by the chiral discrimination factor α_{QCM}, which is defined as (Bodenhofer et al., 1997),

$$\alpha_{\mathrm{QCM}} = \frac{\Delta f_{\mathrm{R}}}{\Delta f_{\mathrm{S}}} \quad \text{or} \quad \alpha_{\mathrm{QCM}} = \frac{\Delta f_{\mathrm{S}}}{\Delta f_{\mathrm{R}}}. \tag{2}$$

The α_{QCM} of enantiomers for the BSA sensor can be ranked in decreasing order: *R*,*S*-TNA (α_{QCM} = 1.34) > *R*,*S*-4-MPEA (α_{QCM} = 1.20) > *R*,*S*-3-MPEA (α_{QCM} = 1.16) ≈ *R*,*S*-2-OT (α_{QCM} = 1.15) > *R*,*S*-MEL (α_{QCM} = 1.11). *R*,*S*-TNA, *R*,*S*-4-MPEA and *R*,*S*-3-MPEA was easily recognized by the BSA sensor. And the α_{QCM} of the HSA sensor can be ranked in decreasing order: *R*,*S*-TNA (α_{QCM} = 1.57) > *R*,*S*-4-MPEA (α_{QCM} = 1.18) > *R*,*S*-2-OT (α_{QCM} = 1.16) > *R*,*S*-MEL (α_{QCM} = 1.13) > *R*,*S*-3-MPEA (α_{QCM} = 1.06). The HSA sensor showed a low chiral discrimination for *R*,*S*-3-MPEA, which can be easily distinguished by the BSA sensor.

3.3. Comparison of the discriminating abilities between BSA and HSA

In order to study the specific discriminating ability between BSA and HSA, the chiral discrimination factors of five pairs of enantiomers on blank gold, BSA and HSA sensors were evaluated. There were same frequency shifts when different *R*- or *S*-enantiomers were introduced onto the blank sensor, while the frequency shifts varied obviously in response to the absorption of enantiomers on both BSA and HSA sensors (Fig. S6, supplementary data). It could be demonstrated that the BSA sensor had higher chiral discrimination for *R*,*S*-4-MPEA and *R*,*S*-3-MPEA. In addition, the HSA sensor showed higher recognition for *R*,*S*-TNA, *R*,*S*-2-OT and *R*,*S*-MEL.

Although the two proteins have similar structures, properties and stereoselectivities, there are obvious differences in separation of large numbers of guests (Allenmark, 1991; Wainer, 1993). Several chiral recognition mechanisms for SA-enantiomer interactions in the gas phase have been proposed. Cavities size or shape fitting is only one of the key factors in chiral discrimination. Other non-covalent interactions also influence the multiple recognition processes by SA, including hydrogen bonding, hydrophobic interaction, electrostatic interaction and Van der Waals interaction. From the three-dimensional structure of HSA, the principal regions of guests binding to HSA were located in hydrophobic cavities in subdomains IIA and IIIA, which were named as Site I and Site II, respectively (He and Cater, 1992).

3.4. Investigation of the interaction between SA and enantiomers

3.4.1. UV–vis spectra

The absorbance of BSA at the peak around 280 nm increased rapidly with increasing concentration of each single *R*- or *S*-TNA, *R*- or *S*-4-MPEA and *R*- or *S*-3-MPEA. In addition, the bindings of the above six single enantiomers to BSA resulted in a slight blueshift towards shorter wavelength. Whereas addition of *R*- or *S*-2-OT and *R*- or *S*-MEL made the peak around 280 nm decreased and there was no shift around the maximal peak (Fig. S7, Supplementary data). Furthermore, the intensity of the two spectra between *R*- and *S*-enantiomers seemed quite different, indicating their different interactions with BSA. Similar UV spectra of HSA with five pairs of enantiomers can be found in Fig. S8 in supplementary data.

The absorption peak around 280 nm of SA can be attributed to aromatic heterocyclic $n \rightarrow \pi^*$ and $\pi \rightarrow \pi^*$ transition of one (HSA) or two (BSA) Trp-residues and nineteen Tyr-residues in the peptide chain (Ulrich, 1981). Addition of TNA, 4-MPEA and 3-MPEA may induce the peptide chain of SA to stretch and the aromatic heterocyclic hydrophobic groups of Trp-residues and Tyr-residues to be exposed. At the same time, the hydrophobic interaction was weakened and the transition energy of $n \rightarrow \pi^*$ and $\pi \rightarrow \pi^*$ was increased, which resulted in a slight blueshift when the complexes was formed. Because the hydroxy (–OH) in 2-OT and MEL can interact with the amino acid residues of SA via hydrogen bonding, the original covalent bonding within the SA amino acid residues would be weakened. As a result, the UV absorption decreased when 2-OT or MEL was added.

All the binding constants K_{A} could be calculated by the modified Hildebrand–Benesi equation (Simard et al., 2006).

$$\frac{1}{A_0 - A} = \frac{1}{K_{\mathrm{A}}} \cdot \frac{1}{C} + I. \tag{3}$$

To define the differences of SA interactions between the two enantiomers, another parameter, UV discrimination factor α_{UV} is suggested as:

$$\alpha_{\mathrm{UV}} = 2\frac{\left|lgK_{\mathrm{R}} - lgK_{\mathrm{S}}\right|}{lgK_{\mathrm{R}} + lgK_{\mathrm{S}}}, \tag{4}$$

Table 1
The binding constant and UV discrimination factor of five pairs of enantiomers to SA.

Enantiomers	Binding constant K_{A} (l mol^{-1})				UV discrimination factor α_{UV}	
	BSA	R^*	HAS	R^*	BSA	HSA
R-TNA	35.15	−0.9999	33.88	−0.9987	0.68	0.71
S-TNA	1399.19	−0.9963	1628.71	−0.9991		
R-4-MPEA	2287.28	−0.9977	1062.7	−0.9999	0.31	0.17
S-4-MPEA	281.69	−0.9997	366.3	−0.9997		
R-3-MPEA	1569.37	−0.9999	1149.43	−0.9998	0.17	0.029
S-3-MPEA	480.77	−0.9987	1409.91	−0.9963		
R-2-OT	40.14	0.9999	66.31	0.9997	0.079	0.14
S-2-OT	30.28	0.9993	37.68	0.9990		
R-MEL	44.50	0.9968	66.67	0.9993	0.049	0.058
S-MEL	37.13	0.9983	52.63	0.9999		

* Regression coefficient.

Table 2
The binding constant and FL discrimination factor of five pairs of enantiomers to SA.

Enantiomers	Binding constant K_a ($l\,mol^{-1}$)				FL discriminating factor α_{FL}	
	BSA	R^*	HSA	R^*	BSA	HSA
R-TNA	14.06	0.9990	45.08	0.9968	0.91	0.86
S-TNA	1122.02	0.9929	14581.43	0.9984		
R-4-MPEA	58884.37	0.9944	6165.95	0.9939	0.49	0.15
S-4-MPEA	794.33	0.9925	1862.09	0.9961		
R-3-MPEA	798.60	0.9928	3090.30	0.9970	0.15	0.017
S-3-MPEA	309.03	0.9951	3548.13	0.9982		
R-2-OT	245.47	0.9947	170.37	0.9992	0.089	0.13
S-2-OT	153.46	0.9998	89.13	0.9966		
R-MEL	398.11	0.9908	439.98	0.9981	0.066	0.065
S-MEL	271.02	0.9969	300.61	0.9991		

* Regression coefficient.

Here K_R and K_S are the UV binding constants of respective enantiomers.

All the binding constants K_A and UV discrimination factors α_{UV} are shown in Table 1. In comparison with the QCM discrimination results, the same trend of chiral discrimination factors was observed, which prove QCM as an effective method in identifying enantiomers.

3.4.2. FL spectra

BSA emits strong intrinsic fluorescence at 349 nm when excited at 280 nm, caused by the Trp-residue located at the 134th and 212th position of the chain. The latter (Trp^{212}) is in the subdomain IIA, which participates in the formation of hydrophobic cavities surface. The hydrophobic cavities play an important role in combining with small molecules, such as chiral molecules (Sulkowska, 2002). When local surroundings altered slightly, the intrinsic fluorescence of BSA would weaken significantly. Protein conformational transition, biomolecule binding and denaturation are responsible for the weakening.

The fluorescence intensity of BSA was obviously weakened with increase in the concentration of ten single enantiomers (Fig. S9, Supplementary data). BSA was not denatured since the experiment was carried out at pH 7.4 and 25 °C. As a result, the possible factors of fluorescence quenching were the alteration of BSA conformation and the binding of *R*- or *S*-enantiomers. The binding interaction would result in fluorescence energy transferring from Trp to *R* or *S* forms, which indicated that the binding site was situated near the Trp^{212}. It was also easy to find differences between *R* and *S* forms. Similar FL spectra of HSA with five pairs of enantiomers can be found in Fig. S10 in supplementary data.

Fluorescence quenching effects usually can be divided into static and dynamic quenching according to the quenching mechanisms. The dynamic quenching is caused by the collision between fluorescent molecules and quenchers, while static quenching is due to the production of non-fluorescence complexes through the reaction of fluorescent molecules and quenchers. If SA fluorescence quenching with enantiomers belongs to dynamic quenching, the process should follow the Stern–Volmer equation (Lakowicz and Weber, 1973).

Therefore, the values of K_q for BSA were calculated and shown in Table S1 in supplementary data All the K_q were larger than the maximum value of collision quenching K_q ($2.0 \times 10^{10}\,l\,mol^{-1}\,s^{-1}$). That indicated that the quenching processes were not mainly caused by dynamic but static quenching mechanisms (Eftink and Ghiron, 1981; Yuan et al., 2007; Du et al., 2009).

The binding constant K_a of *R* or *S* forms can be elicited from the static quenching equation (Alain et al., 1986).

$$lg\frac{F_0 - F}{F} = lgK_a + nlg[Q], \quad (5)$$

where *n* is the number of the binding sites, K_a can be deduced from the intercept of the linear regressions.

The fluorescence discrimination factor α_{FL} is defined in the same manner as UV discrimination factor α_{UV}, and all the data are shown in Table 2. It was obvious that for each pair of enantiomers, the fluorescence discrimination factors α_{FL}, QCM chiral discrimination factors α_{QCM} and UV discrimination factors α_{UV} matched well. Therefore, it is applicable to use the chiral biosensors to recognize different chiral enantiomers.

4. Conclusions

We have successfully constructed QCM chiral biosensors by self-assembled monolayer of SA, which depicted facile and rapid enantioselective recognition. Through the monitoring of the real-time response frequency of five pairs of enantiomers, both SA sensors can be evaluated by QCM discrimination factors. For BSA sensor, the maximum α_{QCM} value was 1.34 (*R*,*S*-TNA) and the minimum was 1.11 (*R*,*S*-MEL), while for HSA sensor, the highest and lowest chiral discrimination factors were 1.57 (*R*,*S*-TNA) and 1.06 (*R*,*S*-3-MPEA). Moreover, the UV and FL spectra have been used to investigate the interactions between SA and enantiomers. The new approach also has applications for more general use in the screening and confirming of appropriate resolving agents for chiral resolution. In addition, since the categories of enantiomers in this study were limited to aromatic and neutral derivatives, further studies are now investigating to recognize more enantiomers such as amino acids and carbohydrates.

Acknowledgments

Financial supports from Natural Science Foundation of China (No. 20771040), Ministry of Education (No. 20071108) and Guangdong Science and Technology Department (No. 2008B050100017) are gratefully acknowledged.

Appendix A. Supplementary data

Supplementary data associated with this article can be found, in the online version, at doi:10.1016/j.bios.2009.06.040.

References

Ahuja, S., 2000. Chiral Separations by Chromatography. Oxford, New York.
Akkerman, H.B., Naber, R.C.G., Jongbloed, B., Hal, P.A., Blom, P.W.M., Leeuw, D.M., Boer, B., 2007. PNAS 104, 11161–11166.
Alain, M., Miehel, B., Miehel, D., 1986. J. Chem. Educ. 63 (4), 365–366.
Allenmark, S., 1991. Chromatographic Enantioseparation: Methods and Applications, 2nd ed. Ellis Horwood, New York.
Bodenhofer, K., Hierlemann, A., Seemann, J., Gauglitz, G., Christian, B., Koppenhoefer, B., Gopel, W., 1997. Anal. Chem. 69, 3058–3068.

Cho, H.M., Jang, D.H., Lee, S.K., Ku, S.J., Kim, H.C., Yu, K.S., Lee, J.W., 2008. Biochip J. 2, 206–211.
Cramer, F, 1994. The Lock and Key Principle. Wiley & Sons, Chichester, UK.
Du, Y.X., Sun, W., Chen, J.Q., Kou, J.P., Yu, B.Y., 2009. J. Lumin. 129, 778–783.
Eftink, M.R., Ghiron, C.A., 1981. Anal. Biochem. 114, 199–277.
Feng, Y.Q., Li, T., Yu, Q.W., Lin, B., 2007. J. Sep. Sci. 30, 804–812.
Fung, Y.S., Wong, Y.Y., 2001. Anal. Chem. 73, 5302–5309.
He, X.M., Cater, D.C., 1992. Nature 358, 209–215.
Inagaki, S., Min, J.Z., Toyo'oka, T., 2008. Anal. Chem. 80, 1824–1828.
Jacinto, S., Johanna, K., Joan, G.L., 1971. Biochemistry 10, 4005–4098.
Kim, W.S., Guo, H.S., Kim, J.M., Chang, S.M., 2009. Biosens. Bioelectron. 24, 2931–2934.
Kragh-Hansen, U., Chuang, V.T.G., Otagiri, M., 2002. Biol. Pharm. Bull. 25, 695–704.
Lakowicz, J.R., Weber, G., 1973. Biochemistry 12, 4161–4170.
Li, Y., He, W.Y., Liu, H.X., Yao, X.J., Hu, Z.D., 2007. J. Mol. Struct. 831, 144–150.
Malhotra, B.D., Arya, S.K., Solankia, P.R., Dattab, M., 2009. Biosens. Bioelectron. 24, 2810–2817.
Ng, S.C., Chan, H.S.O., Xu, C.H., 2008. Langmuir 24, 9118–9124.
Sadik, O.A., Aluoch, A.O., Zhou, A., 2009. Biosens. Bioelectron. 24, 2749–2765.
Silien, C., Buck, M., Goretzki, G., Lahaye, D., Champness, N.R., Weidner, T., Zharnikov, M., 2009. Langmuir 25, 959–967.
Simard, J.R., Zunszain, P.A., Hamilton, J.A., Curry, S., 2006. J. Mol. Biol. 361, 336–351.
Storri, S., Santoni, T., Minunni, M., Mascini, M., 1998. Biosens. Bioelectron. 13, 347–357.
Sulkowska, A., 2002. J. Mol. Struct. 614, 227–232.
Ulrich, K.H., 1981. Pharmacol. Rev. 33, 17–53.
Wainer, I.W., 1993. Drug Stereochemistry: Analytical Methods and Pharmacology, 2nd ed. Marcel Dekker, New York.
Ward, T.J., 2000. Anal. Chem. 72, 4521–4528.
Wei, S.L., Song, G.Q., Lin, J.M., 2005. J. Chromatogr. A 1098, 166–171.
Yuan, J.L., Lu, Z., Liu, Z.G., Hu, Z., Zou, G.L., 2007. J. Photochem. Photobio. A 191, 104–113.